2020-05-10

Exoskeleton dissolution with mechanoreceptor damage in larval Dungeness crab related to severity of present-day ocean acidification vertical gradients

Bednarsek, N

10.1016/j.scitotenv.2020.136610
Science of The Total Environment
Elsevier BV

Exoskeleton dissolution with mechanoreceptor damage in larval Dungeness crab related to severity of present-day ocean acidification vertical gradients

Authors: Nina Bednaršek[1], Richard A. Feely[2], Marcus W. Beck[1], Simone R. Alin[2], Samantha A. Siedlecki[3], Piero Calosi[4], Emily L. Norton[5], Casey Saenger[5], Jasna Štrus[6], Dana Greeley[2], Nikolay P. Nezlin[1], Miranda Roethler[1], John I. Spicer[7]

Affiliations:

[1]Southern California Coastal Water Research Project, Costa Mesa, CA, 92626 USA

[2]NOAA Pacific Marine Environmental Laboratory, 7600 Sand Point Way NE, Seattle, WA, 98115 USA

[3]Department of Marine Sciences, University of Connecticut, Groton, Connecticut 06340

[4]Département de Biologie, Chimie et Géographie, Université du Québec à Rimouski, 300 Allée des Ursulines, Rimouski, QC G5L 3A1, Canada

[5]Joint Institute for the Study of the Atmosphere and Ocean, University of Washington, Seattle, WA, 98195 USA

[6]Department of Biology, Biotechnical Faculty, University of Ljubljana, Ljubljana, Slovenia

[7] University of Plymouth, School of Biological and Marine Sciences, Plymouth PL4 8AA, UK

***Corresponding author:** Nina Bednaršek (ninab@sccwrp.org); (714) 755-3237

Running title: Dungeness crab sensitivity to acidification

Keywords: Dungeness crab, larval sensitivity, global climate change, ocean acidification, exoskeleton structure, dissolution, mechanoreceptor damage.

Abstract:

Ocean acidification (OA) along the US West Coast is intensifying faster than observed in the global ocean. This is particularly true in nearshore regions (< 200 m) that experience a lower buffering capacity while at the same time providing important habitats for ecologically and economically significant species. While the literature on the effects of OA from laboratory experiments is voluminous, there is little understanding of present-day OA *in-situ* effects on marine life. Dungeness crab *(Metacarcinus magister)* is perennially one of the most valuable commercial and recreational fisheries. We focused on establishing OA-related vulnerability of larval crustacean based on mineralogical and elemental carapace to external and internal carapace dissolution by using a combination of different methods ranging from scanning electron microscopy, energy dispersive X-ray spectroscopy, elemental mapping and X-ray diffraction. By integrating carapace features with the chemical observations and biogeochemical model hindcast, we identify the occurrence of external carapace dissolution related to the steepest Ω calcite gradients ($\Delta\Omega_{cal,60}$) in the water column. Dissolution features are observed across the carapace, pereopods (legs), and around the calcified areas surrounding neuritic canals of mechanoreceptors. The carapace dissolution is the most extensive in the coastal habitats under prolonged (1-month) long exposure, as demonstrated by the use of the model hindcast. Such dissolution has a potential to destabilize mechanoreceptors with important sensory and behavioral functions, a pathway of sensitivity to OA. Carapace dissolution is negatively related to crab larval width, demonstrating a basis for energetic trade-offs. Using a retrospective prediction from a regression models, we estimate an 8.3% increase in external carapace dissolution over the last two decades and identified a set of affected OA-related sublethal pathways to inform future risk assessment studies of Dungeness crabs.

Introduction

Since the pre-industrial era, anthropogenic CO_2 uptake along the US West Coast have resulted in rapid intensification OA rate on a global scale (Chavez et al., 2017; Feely et al., 2016), resulting in lower carbonate conditions compared to the pre-industrial times. This is because of the low regional buffering capacity, which contributes to low pH and carbonate mineral saturation states for both aragonite (Ω_{ara}) and calcite (Ω_{cal}) (Feely et al., 2018). These changes in carbonate chemistry have resulted in in substantially reduced habitat suitability for marine calcifiers (Bednaršek et al., 2014; Somero et al., 2015). These findings are supported by the field and synthesis work along the North American Pacific demonstrating that calcifying invertebrates will be the ones most impacted by progressive OA (Bednaršek et al., 2017; Busch & McElhany, 2016). Apart from evidence of OA impacts on pteropods and other calcifiers caused by the low Ω_{ara} conditions in upwelling systems (Bednaršek et al., 2014, 2017) and around CO_2 vent seeps and sites (Manno et al., 2019; Tunnicliffe et al., 2009), there is limited understanding of present-day OA effects on marine life *in situ*. That is especially relevant for the crustaceans since they were considered less sensitive to OA parameters (like pCO_2 or pH) after studies demonstrated their capacity to abate initial hypercapnia and to buffer extracellular acid-base disturbances (Melzner et al., 2009; Pane and Barry, 2007) with limited or no change in aerobic metabolism (Paganini et al., 2014). However, restoring internal pH to sustain physiological and biogeochemical processes (Somero, 1986), typically requires activation of buffering, which is energetically expensive process (Cameron, 1985; Michaelidis et al., 2005). Recent experimental findings have demonstrated increased sensitivity to OA-related stressors in crustaceans, especially in the early life stages that can be regarded as a potential bottleneck for the population level responses (Schiffer et al., 2014; Small et al., 2015). Regardless of the

habitats that different species inhabit, the studies investigating OA effect on larval stages reported lower growth and decreased survival of blue crab (Giltz and Taylor, 2017), delayed metamorphosis in the stone crab (Gravinese et al., 2018), changes in exoskeleton composition (Page et al., 2016) and decreased metabolisms in Tanner crabs (Long et al., 2016) and increased energetic costs in the porcelain crab (Carter et al., 2013), while the pre-larval of the Dungeness crab showed reduced survival and slower progression through the development (Miller et al., 2016). With annual revenues up to $220 million (Hodgson et al., 2018; Pacific States Marine Fisheries Commission, 2019), the Dungeness crab (*Metacarcinus magister*) is one of the most valuable and recreational fisheries in the US coastal waters. Terminal stage of pelagic Dungeness crab larvae (megalopae) undergoes long distance transport along the north Pacific coast of North America before settling in suitable benthic settlement site (Shanks, 1995; Sinclair, 1988). Given their diel vertical migration extends down to 60 m depth (Hobbs et al., 1992), megalopae encounter steep vertical pH, Ω_{cal} gradients in coastal habitats; however, the duration and magnitude of their exposure to these conditions remains largely unknown despite the exposure history notably impacting organismal responses (*sensu* Bednaršek et al. (2017).

To start addressing potential OA vulnerability of the pelagic Dungeness larvae *in situ*, their spatial distribution must be paired with *in situ* exposure history (as defined in Bednaršek et al., 2017), understanding of their physiological susceptibility and their structural and mineralogical features. In regards to the later, surprisingly little is known about these features that can predispose an individual to extensive exoskeleton dissolution if the conditions in the external environment are conducive for it. In addition, for detecting environmental clues, the decapod exoskeleton contains elongated hair-like structures called setae, which are important chemo- and mechanoreceptors involved in sensory and behavioral responses. While the

lipoproteic epicuticle-covered exoskeleton consists of two cuticular mineral carbonate layers (Chen et al., 2008) (i.e., the outer exocuticle and the inner endocuticle) in the Dungeness crab adults such structure or its composition is completely unknown for the larvae.

This interdisciplinary study integrates physical, geochemical, biological, and modelling components across the individual and population-level parameters. Identification of the carapace crystalline mineralogical and elemental composition provided an understanding behind the extensive exoskeleton dissolution and mechanoreceptor damage. The latter was linked with the chemical observations made along the North American West Coast to identify the drivers and OA hotspots of *in situ* megalopae vulnerability. The biogeochemical model hindcast was used to determine the impact of *in situ* exposure history in the coastal habitats.

Materials and methods

Carbonate chemistry, sampling and analyses

For the purpose of this study, the NOAA West Coast Ocean Acidification (WCOA) cruise in May–June 2016 sampled conductivity, temperature, depth, and oxygen. Data on the conductivity, temperature, and pressure of seawater (CTD) were collected along cross-shelf transects, accompanied by biological stations with vertical sections of temperature (T), salinity, nutrients, oxygen, chlorophyll-a (chl-a), dissolved inorganic carbon (DIC), total alkalinity (TA), spectrophotometric pH (measured at 25°C and corrected to *in situ* temperatures, and expressed on the total pH scale, subsequently expressed pH_T). pCO_2 and calcite saturation state (Ω_{cal}) were calculated using CO2SYS as described by Feely et al. (2016) and Bednaršek et al. (2012). Larvae were collected using Neuston and Bongo nets with a mesh size of 333 μm, which were deployed

in an oblique manner at 10 stations during the night in the upper surface waters, an area that encompasses the nocturnal vertical habitat of larval Dungeness crabs of the upper 60 m (Hobbs et al., 1992; Morgan, 1985), with the following environmental parameters along the vertical habitat (Table S1). The duration of tows was 15–20 min. Megalopae were identified and then stored in 100% non-denatured ethanol, and also flash-frozen at -80 °C for later comparison of two different preservation methods.

Using SEM methods to detect and evaluate carapace dissolution

Megalopae carapaces were investigated using a combination of different methods: 1) scanning electron microscopy (SEM; Hitachi Phenom, USA) to determine potential structural changes on the cuticular surface; 2) energy dispersive X-ray spectroscopy (EDXS at the University of Washington) for mineralogical composition; 3) elemental mapping; and X-ray diffraction (University of Washington and Max Planck Institute) for elemental content across mostly lipoproteic carapace (Figure S1, Fig. 1). Here, we define exoskeleton as the cuticle covering the dorsal part of the carapace of the larval crab, and five pereopods, with chelae. The carapace epicuticle, which otherwise overlies the crystalline layer and makes dissolution observations impossible, was removed from each megalopa prior to analysis. This was accomplished using sodium hypochlorite, which efficiently removes the epicuticle but does not damage the crystalline layers underneath, even at high concentrations (Bednaršek et al., 2012). On the samples with no hypochlorite treatment, the epicuticle covered the crystalline layer so no investigation of dissolution was possible. Therefore, we tested different concentrations and duration of hypochlorite treatment on the individuals from the same station to ensure that we fully removed the epicuticle, without triggering dissolution of the calcite crystalline layers beneath it. The combination of 1 and 3 % sodium hypochlorite with 15, 30, and 120 min

136 treatments only partially removed the epicuticle, , while 6% hypochlorite treatments for 4 and 6
137 hours were effective in epicuticle removal, without inducing additional dissolution at the longer
138 duration.

139 To determine the treatment does not induce any damage, we have tested the individuals from the
140 same stations with different combination of treatments. We assumed the similarity of exposure
141 history of individuals within the same stations (see modelling section). The results of no
142 difference in dissolution under the different combination of concentration/duration of treatment
143 combination was a confirmation that the treatment did not induce any additional damage, and
144 thus did not confound our field observations.

145 We determined 6% hypochlorite for 3-4 h to be an efficient and effective treatment, similar to
146 the treatment previously described for the removal of the periostracum in pteropods (Bednaršek
147 et al., 2012). After soaking in sodium hypochlorite, samples were rinsed several times in
148 Millipore water to remove any organic matter remaining on the surface of the exoskeleton. It is
149 important to note that when examining the presence of setae within the neuritic canals, we did
150 not use any treatment in order to avoid any methodological artifacts. When examining the
151 internal area of the cuticle, we avoided examining the proximity of the gills given that
152 dissolution could be impacted by the processes around. To quantify the dissolution of internal
153 carapace cuticle, the pereopods and soft tissue of larvae were gently removed from the rest of the
154 body and washed in Millipore water to remove any remaining tissue or organics before treatment
155 with sodium hypochlorite. Each of the five pereopod cuticle was examined across the proximal
156 and distal ends, with particular focus on chelae (Figure S2). SEM was used to evaluate the extent
157 and severity of dissolution. We focused on three distinct features: ridging structures, dissolution
158 around setae, and exposed calcite crystals (Figure S2, S3).

159 For estimating the various body parameter change (in mm) of larvae across various
160 vertical OA gradients, we have measured carapace length (CL), total length from rostrum to
161 telson (TL), length from rostrum to dorsal carapace spine (R-DCS), and carapace width (CW).
162 The CW is the most commonly used parameter by various US federal agencies along the US
163 West Coast to regulate crab management catch efforts (Davis et al., 2017). Here, we assume that
164 all the larvae were released at the same time to allow for body parameter comparisons across
165 different stations. Using the methodology to characterize the megalopae stages by González-
166 Gordillo et al. (2004), we determined that all megalopae were in the intermolt stage, except for
167 those from Station 115, which were transitioning into the premolt stage. We excluded the results
168 of the internal dissolution observations from this station in case promoting process changed any
169 features on the internal side that could bias accurate dissolution assessment.

170 ***Semi-quantitative dissolution assessment***

171 Altogether, we analyzed 50 individuals from 10 environmental stations across OA-related
172 vertical gradients of varying strength. We used 3–5 individuals per station to determine
173 dissolution extent of the external side of carapace cuticle, as well as the cuticle of the pereopods.
174 We used an additional 2–3 individuals per station to analyze the internal side of the cuticle.
175 Approximately 10–20 SEM images were produced per individual on the external and internal
176 sides, with the images being manually examined to detect any signs of dissolution. For crystal
177 exposure characterization, the same categorization of dissolution conditions as previously
178 described in pteropods was used (Bednaršek et al., 2012). We identified three major features of
179 exoskeleton dissolution and developed a categorization scheme for all three features, showing
180 them in their intact forms (Stage 0, Figure S2) and progressively altered forms (Stage 1 and 2;
181 Figure S1; Table S2). These features differentiated damaged surfaces from the intact surfaces

(Table S2). The cuticular surface of the carapace and the pereopods under high Ω_{cal} *in situ* conditions had a smooth, sleek appearance (Figure S2; Stage 0). At greater magnification, individual calcite crystals were visible in these areas (Figure S2). Signs of dissolution tended to be more prevalent and more severe on the surface immediately surrounding setae pores. Consequently, areas around the setae were considered separately from the rest of the exoskeleton. From these observations, a semi-quantitative scoring metric was developed based on previous work on pteropods and used to score the remainder of the samples. For each sample, the three separate features (presence and depth of ridge structures, exposure of individual calcite crystals, and the prevalence of dissolution features around setae pores) were each assigned a score. The features were scored on a scale of 0 to 1 based on the severity of dissolution: intact exoskeleton with no dissolution received a score of 0; moderate dissolution received a score of 0.5; and substantial dissolution of all examined features was scored 1 (Figures S1–S3). Since the crab exoskeleton of the carapace and pereopod differ in their chemical composition, these three areas were assigned separate scores. Because of the surface analyses required separately for the external and internal dissolution, both types of analyses could not be conducted on the same individual. All three features displayed similar trends, so the scores were averaged to unitless 'relative dissolution', describing internal and external dissolution. Observation of setae presence/absence was included in the exoskeleton observation under SEM on intact specimen before any preparation treatments were conducted to eliminate the possibility of preparation steps affecting setae presence or outrooting them from the carapace.

Mineralogical analyses

The mineralogy of selected megalopae was characterized using X-ray diffraction (D8 Discover 2D; University of Washington, Seattle). Prior to analysis, carapaces from five megalopae at each

site were coarsely crushed and treated for 10 min using a dilute (3%) sodium hypochlorite solution to minimize interference from organic matter but without compromising mineralized structures. Samples were dried completely and then ground to a fine homogenous powder representing the aggregate of the five individuals from each location. Resulting diffractograms were compared to a catalog of mineral-specific patterns to constrain the primary mineralogy of each sample.

Elemental analyses

We used energy-dispersive X-ray spectroscopy (EDXS) to estimate elemental composition of the carapace and pereopod cross-sections (N = 7) from samples across different natural OA vertical gradients over spatial scales. For elemental analyses, we have not removed the epicuticle from the samples. These gradients analyses were conducted at Max Planck Institute for Marine Microbiology in Bremen, Germany. Prior to analyses, we dehydrated samples using 100 % ethanol and dried them in a critical point dryer. We prepared the sections by fracturing different carapace regions which was followed by the EDXS investigations (Figure 1).

Statistical analyses

Biological measurements from Dungeness megalopae collected at 10 stations along the North American Pacific Coast (Figure 2) were paired with synoptic environmental data from CTD profiles. Environmental data were summarized as depth-integrated averages from the surface to the maximum depth of each CTD profile to characterize the exposure conditions in the upper water column. In addition, $\Delta\Omega_{cal,60}$ was estimated as the difference from the observed measurement at each depth bin with that of the surface. This measurement characterized the relative Ω_{cal} gradients with increasing depth and accounted for differences in the relative

magnitudes of Ω_{cal} between stations. Chlorophyll-a observations were highly skewed and so were log-transformed prior to analysis.

Biological responses included dissolution, body parameter, and abundance with various environmental vertical gradients to identify significant associations using generalized linear models. For comparison of the biological data to environmental conditions, each depth bin for the depth-integrated values was evaluated to identify at which depth associations between biological response and selected environmental variables were strongest. In addition, carapace dissolution was compared to body parameters to characterize potential linkage between the physiological parameters, growth, and population-level effects (abundance). Comparisons of biological measures to each other were also accomplished with generalized linear models.

Gaussian distributions were assumed for all response variable models, excluding presence/absence, which was modeled using a binomial logistic response curve. Models and individual parameters were considered significant at $\alpha = 0.05$. All models had N = 10 except presence/absence models with N = 24, which included additional stations where tows were conducted but no crabs were found. Finally, all variables were evaluated together to identify pairwise associations using Pearson correlation analysis and redundancy analysis (RDA) to characterize how the biological response measures were jointly explained by the environmental variables. For the latter analysis, all input data were standardized to range from 0 to 1 to account for differences in scale between variables. The *vegan* package for the R statistical programming language was used for standardization and RDA (Oksanen et al., 2019; R Core Team, 2019).

For selected predictors, additional models were developed to evaluate the additive effects of two predictors on dissolution. Backward model selection was used to identify the most parsimonious model by sequentially dropping individual predictors and comparing Akaike

Information Criterion values (AIC) (Akaike, 1973; Fox and Weisberg, 2011). This allowed us to determine if there was any additional power in combining predictors to explain dissolution, or consequently, if dissolution could be sufficiently explained using only one predictor. For example, the ability of both Ω_{cal} and chlorophyll to explain dissolution were evaluated to better understand the relative effects of both.

J-SCOPE model outputs of the larval exposure history prior to sampling

The Joint Institute for the Study of the Atmosphere and Ocean (JISAO)'s Seasonal Coastal Ocean Prediction of the Ecosystem (J-SCOPE, http://www.nanoos.org/products/j-scope/) features dynamical downscaling of regional ocean conditions in Washington and Oregon waters (Siedlecki et al., 2016). Model performance and predictability examined for sea surface temperature (SST), bottom temperature, bottom O_2, pH, and Ω_{ara} through model hindcast, reforecast, and forecast comparisons with observations, showing significant measurable skill on seasonal timescales (Kaplan et al.2016; Siedlecki et al., 2016; Norton et al., *in revision*)**.** Megalopae exposure histories were simulated by releasing 100 representative particles, with vertical migration behavior over 60 m inserted into the predicted circulation field at each of the *in situ* sampling locations and times, and then tracking them backward in time for 30 d following methods described for pteropods in Bednaršek et al. 2017, and for megalopae in Norton et al., *in revision*. The vertical migration behavior was simulated using the LTRANSv2b larval transport model (North et al., 2008, 2011; Schlag and North, 2012) that has recently been implemented in the J-SCOPE system and adapted for megalopae (Norton et al., *in revision)*.

Results

272 ***Elemental and crystalline characterization of the carapace***

273 The compilation of our results demonstrate that the carapace is highly mineralized and
274 precipitated into a chitin-proteinaceous matrix. XRD identify calcite as a primary polymorph in
275 the carapace. The mineralized exoskeleton of the megalopae intermolt stages consists of the
276 thinner exocuticle on the surface that is less than 2–3 μm thick, and the thicker and more
277 compact endocuticle underneath (Figure 1) of approximately 6–7 μm, with the combined
278 thickness up to 10 μm. The carapace surface is extensively covered with setae that are rooted in
279 the calcified neuritic canals each with an average of about 5 μm surface opening (Figures S2 and
280 S3). EDXS investigations characterized detailed elemental structure with average Ca^{2+} content of
281 28 % in the carapace and pereopods, with much higher Ca^{2+} found within in the mid layer and
282 the endocuticle (higher than 50%) compared to less than 20% found in the exocuticle (Figure 1).
283 The carapace endocuticle contains also a high concentration of Mg^{2+} with some areas of the
284 carapace exceeding 5% content, categorizing it as a more soluble high-Mg calcite. In addition,
285 the internal side contain high concentrations of phosphorus (up to 6%) and strontium (up to 2%)
286 on the inner endocuticle (Figure 1). The percentage of different dissolution features is similar
287 between the carapace and the pereopods, however with much less variation in all elements
288 between the carapace and pereopods (Figure S1). This elemental composition indicates that other
289 crystalline forms of carbonate could be precipitated into a chitin-proteinaceous matrix, such as an
290 amorphous calcium carbonate (ACC) crystalline layer, but the methods used were not suitable
291 for ACC detection. The strong presence of autofluorescence prevented more precise detection of
292 any other crystalline forms, despite extensive use of Raman spectroscopy for this purpose.
293 Nevertheless, such elemental structure resembles a layer of ACC with Mg^{2+}, phosphate and

carbonate-rich phase, or ACC with magnesian calcite, as previously demonstrated in the edible crabs *Cancer pagurus* (Fabritius et al., 2012).

Megalopae habitat characterization with strong vertical and spatial Ω_{cal} vertical gradients

Crab megalopae were found in both outer-shelf, slope, as well as nearshore (<200 m depth) habitats, with distinctly different vertical environmental gradients in the upper water column. Due to the upwelling of deeper, colder, CO_2-rich waters in the near-shore and coastal habitats, steep gradients in low pH and Ω_{cal} values were observed. In comparison, offshore region were characterised with more uniform vertical gradients with lower vertical difference were over the same depth interval (Figure 2). Pronounced steep OA-related vertical habitats were observed in the upper 60 m of the water column, here represented as the difference between the surface and 60 m depth ($\Delta\Omega_{cal,60}$ or ΔpH_{60}), which is within the lower range of megalopae diel vertical migration habitat. Among all tested depths, statistical models comparing biological responses (e.g. exoskeleton dissolution, body parameters, abundance) with environmental conditions had the strongest associations using the 60 m vertical depth integrated value (e.g., external dissolution on body parts vs. $\Delta\Omega_{cal}$ had the highest R^2 = 0.821 at 60 m). Hereafter, all environmental data are reported using the 60 m depth integrated values. Coastal conditions recorded near-saturation Ω_{cal} values down to 1.4, pH down to 7.48, and pCO_2 up to 910 uatm (Table S1; Figure 2).. There were no observations of $\Omega_{cal} < 1$ or hypoxia, with similar oxygen ranges observed in the onshore and offshore regions, while average temperature that was by about 1.3° C warmer offshore. Food availability was an order of magnitude higher in the onshore regions compared to offshore, with the highest chl-a values recorded at 25 $\mu g\ L^{-1}$ (Figure 2).

316 Multiple environmental parameters co-varied (Figure 3a) as observed in the RDA plot at
317 60 m depth (Figure 3b). The first two axes of the RDA explained approximately 90% of the
318 variation among the biological and environmental parameters. The first RDA axis was
319 characterized by a $\Delta\Omega_{cal,60}$ vertical gradient and external dissolution, with both having negative
320 loadings along the RDA1 axis. Carapace width was negatively correlated with $\Delta\Omega_{cal,60}$, whereas
321 external dissolution was positively correlated, suggesting that larger individuals had less
322 dissolution and were associated with lower gradients in $\Delta\ \Omega_{cal,60}$. While OA parameters (pCO_2,
323 pH) were all correlated as indicated by alignment with the second RDA axis, the collinearity
324 with temperature was not significant. We found less collinearity among the environmental
325 parameters related to the 60 m vertical gradients, such as $\Delta\Omega_{cal,60}$, $\Delta O_{2,60}$, and ΔT_{60}. Here, we
326 focused on the mechanistic drivers that are explicitly involved in the external dissolution
327 processes, we have examined $\Delta\Omega_{cal,60}$ in how it relates to external dissolution. Similarly, internal
328 dissolution was negatively correlated with pCO_2 along the second axis with slightly higher
329 loading along the RDA1, and also slightly negatively related with increased temperature. The
330 implications of this association and how they related to model output (Figure 7) will be
331 explained below.

332 ***Megalopae carapace dissolution and reduced width as responses to variable OA parameters***
333 ***across vertical scales***

334 Dissolution assessment on the external surface of the exocuticle and internal surface of the
335 endocuticle of the megalopa's carapace and pereopod exoskeleton, was conducted only after
336 confirming that sample preservation did not impact dissolution patterns, i.e. samples preserved in
337 ethanol vs. flash frozen did not exhibit any significant difference in their dissolution features.
338 Using a novel categorization scheme to semi-quantify dissolution features, including ridging

structures, dissolved areas around neuritic canals, and exposed calcite crystals (Figures 4, S1 and S2; Table S2), the individuals demonstrated various extents of these features present on the external side of the carapace and the pereopod exoskeleton (Figure S2 and S3). On the carapace, the front and outer surfaces were the most affected (Figures 4 and S3). On the pereopod exoskeleton, the thoracic segments and chelae had the most severe dissolution, while the distant parts were less affected (Figure S3). On all of the examined individuals with external dissolution, we also found evidence for internal endocuticle dissolution, which was, on average, approximately half that observed on the external exocuticle surface.

Average dissolution on the exocuticle showed the strongest linear dependence with $\Delta\Omega_{cal,60}$ (Figure 5; $R^2 = 0.866$, $p < 0.001$), demonstrating that the habitats with the steepest 60 m vertical gradients results in the most damaged organisms. Because of the topographic features, there is a spatial variability related to the occurrence of the steepest $\Delta\Omega_{cal,60}$ gradients, meaning that the lowest exoskeleton dissolution does not always correspond to the offshore gradients.

The internal dissolution showed the most robust evidence, though not statistically significant, of correlation with pCO_2 values (Figure 5; $R^2 = 0.406$, $p = 0.065$) and negative marginal significance with temperature ($R^2 = 0.435$, $p = 0.053$). The internal dissolution rapidly intensified beyond pCO_2 >500 μatm (Figure 5b), with this being a robust threshold. There was no significant correlation between internal and external dissolution (Figure 5; $p = 0.18$), suggesting decoupling of the two processes.

At sites with a small $\Delta\Omega_{cal,60}$, the external surface of the carapace was characterized by predominantly smooth surfaces, the absence of dissolution, and the presence of setae (Figures 7 and S2). Ridging features were present on all examined carapaces but significantly increased at the stations with the greatest $\Delta\Omega_{cal,60}$ difference (Figures 4 and 5). This presence of ridging

features co-occurred with the increased occurrence of crystal exposure, ranging from increased porosity (Stage 1) to exposed crystals (Stage 2) at the sites with lower $\Delta\Omega_{cal,60}$ difference, and deeper-protruding dissolution at the sites with greater $\Delta\Omega_{cal,60}$ difference (Stage 2). Using image analysis, the depth of ridging structures was estimated at approximately 2 μm, around 25% of the cuticle thickness. Given the exocuticle thickness of 2–3μm, the dissolution extended into the endocuticle (Figure 6). The extent of dissolution on pereopod exoskeleton was comparable with the external dissolution, especially at the higher dissolution values (Figure S5; $R^2 = 0.65$; $p = 0.0047$, slope = 0.901), indicating that both features were reliable metrics for dissolution assessment.

There was a distinct pattern of severe dissolution specifically developed around the calcified neuritic canals (Figure 6). In megalopae collected at inshore stations (< 200 m bottom depth), the carapace surface around the neuritic canals was markedly dissolved (Stage 2), and mechanoreceptors were often absent. Dissolution around the neuritic canals appeared to alter the morphology of the setae (Figure 6). Setae edges were partially collapsed at the places where the mechanoreceptors are anchored in, with the initial ridging features around the canals degenerated into severely dissolved surfaces at the more intense $\Delta\Omega_{cal,60}$ values (Figure 6). On the megalopae from offshore stations with a smaller $\Delta\Omega_{cal,60}$ the mechanoreceptors were present with no damage around the neuritic canals and less severe dissolution. Within the region of altered setae, dissolution up to 2–3 μm around the setae (Figure S4) was accompanied by significant canal deformation. This deformation appears to destabilize the attachment of the setae anchor, resulting in the setae ‘outrooting’. In some of the calcified neuritic canals, we noted the absence of setae but have not yet quantified the frequency of this occurrence.

384 To examine whether external or internal dissolution affects organismal or even
385 potentially population-level metrics, dissolution measures were compared to megalopae body
386 parameters and abundance. Here, we made an assumption that all the larval were released at the
387 same time to be able to compare different length parameters. We detected a significant negative
388 correlation between external dissolution and width, as indicated by reduced individual carapace
389 width (CW; $F = 18.61$, $R^2 = 0.823$, $p = 0.013$ for the regression of CW against external
390 dissolution on body parts; $F = 5.3$, $R^2 = 0.57$, $p = 0.08$ for the regression of CW against all
391 external dissolution; Figure 5d), which is particularly strong in the coastal stations. This
392 demonstrates that external OA-related exposure can indirectly result in reduced larval width.
393 Carapace width was strongly oriented along the first RDA axis (Figure 3), while being
394 orthogonal to internal dissolution and directly opposed to external dissolution. The latter aligns
395 with previous findings that internal dissolution is uncoupled from carapace width (linear model p
396 > 0.05), whereas external dissolution is significantly associated with carapace width (RDA plot).
397 Other length-related parameters (CL, R-DCS, TL) were not affected by OA parameters,
398 demonstrating that only specific body parameters, i.e., width are affected at more severe $\Delta\Omega_{cal,60}$
399 vertical gradients.

400 On the higher, population-level response, only chl-a was found to be a significant driver.
401 Abundance was positively correlated with chl-a at 60 m depth for both onshore and offshore
402 habitats ($R^2 = 0.327$; $p = 0.008$). None of the other environmental parameters had a significant
403 impact. However, in shallow coastal habitats with depth <30 m, temperature was negatively
404 related to larval abundance (for temperature at 10 m, $R^2 = 0.241$; $p = 0.02$; $F = 6.56$), although
405 chl-a remained the dominant driver. In addition, neither carapace dissolution nor the width was

related to larval abundance, suggesting decoupling of individual- and population-level effects of environmental conditions on larval Dungeness during the present day.

Megalopae exposure history to coastal OA conditions during the month prior to sampling

Particle back-tracking results with simulated vertical migration between the ocean surface and 60 m depth over a 30-d period from the J-SCOPE simulations showed that megalopae that were released in coastal habitats (<200 m), remained in coastal habitat for nearly a month of simulation regardless of their position in the domain (Figure 7). This retention results in extended exposure to steeper coastal vertical gradients in OA conditions (Figure 2), and consequently, more intense dissolution (Figure 5).

Discussion

To our knowledge this is the first time that OA-related dissolution of calcite structures *in situ* has been demonstrated for crustaceans. Our results indicate that it is the exposure to both parameters, $\Delta\Omega_{cal,60}$ (i.e. the difference in calcite saturation depth between the surface and 60 m depth) and pCO_2, set up by as well as prolonged (<1 month) retention in the coastal waters that characterizes the suite of *in situ* parameters determining the larval crab vulnerability. This primarily demonstrates that it is not just the mean state OA conditions, but also the vertical difference in the water column that can induce negative biological responses. Using a retrospective prediction from a regression model (Figure 5a), we estimate an 8.3% increase in the extent of external carapace dissolution over the last two decades. This post-hoc estimate was based on a ΔpH changes of 0.02 unit per decade (Carter et al., 2018), comparing current average with the extent of dissolution predicted from our regression model based on the *in situ* observations (Figure 5a with the equation in the figure content) by using the estimated pH conditions two decades prior.

This is a reasonable estimate since $\Delta\Omega_{cal,60}$ is highly correlated with $\Delta\Omega_{pH,60}$ ($F = 204.3$, $R^2 = 0.96$, $p < 0.001$, Figure S6).

What makes this OA-dependent dissolution of megalopae particularly relevant is that the crab samples originated in the supersaturated conditions with respect to calcite (the lowest Ω_{calc} =1.41). Since the dissolution reported in other calcifiers has been demonstrated above Ω_{ara} of 1.4–1.5 (Bednaršek and Ohman, 2015; Bednaršek et al., 2016), we conclude that exoskeleton dissolution is initiated at higher $\Delta\Omega_{cal,60}$ than predicted based on thermodynamic principles alone. Furthermore, using exposure metrics based on the biogeochemical model output demonstrates that 1-month long exposure in coastal habitats with large $\Delta\Omega_{cal,60}$ values can result in significantly more dissolution than predicted based on snap-shot observational data. In comparison with the chemical observations, particle tracking model output indicates prolonged severity of exposure to the coastal low OA conditions, allowing for more extensive exoskeleton dissolution and reduced larval width in those habitats. It is worth noting that dissolution could be viewed as a physiological strategy to compensate against unfavorable external conditions. Dissolution of the outer calcite layer could increase the release of the bicarbonate and hydroxyl ions, raising pH, and providing a rapid alkalinization of the superficial layer (Kunkel et al., 2012). This alkaline layer could then provide an additional local protection from exposure to a large $\Delta\Omega_{cal,60}$ conditions by blocking protons from continuously invading the internal fluid However, as the larvae live in highly dynamic environments, such a layer would be continuously disrupted, explaining the high extent of external dissolution.

Dissolution as a mechanism to offset OA-related extracellular acid-base disturbance?

Species with a developed capacity for ion exchange to maintain extracellular acid-base balance, are able to compensate for the effects of exposure to high pCO_2 waters and restore extracellular

451 pH values optimal for physiological and biogeochemical processes (Somero, 1986). They do so
452 via energetically expensive buffering of intra- and extracellular compartments achieved through
453 various mechanisms, such as buffering by seawater-derived bicarbonate sources (Truchot, 1979),
454 and increased respiratory activity to reduce CO_2 loading of the extracellular fluid and non-
455 bicarbonate buffering (Cameron, 1985; Hans et al., 2014; Michaelidis et al., 2005).

456 However, the downside to the well-established extracellular acid-base control is an energetically
457 demanding process (Hans et al., 2014; Michaelidis et al., 2005; Pane and Barry, 2007; Trigg et
458 al., 2019). Therefore, we hypothesize that the internal carapace dissolution we observed in our
459 study could be a part of a passive ability to buffer reductions in extracellular pH, a feature found
460 in a variety of marine invertebrates including bivalves, echinoderms, and crustaceans (Cameron,
461 1985; Henry et al., 1981; Lindinger et al., 1984; Spicer and Taylor, 1987; Spicer et al., 2007).
462 The narrow neuritic canals around the mechanoreceptors allow communication through secretion
463 across the internal-external cuticle layers (Kunkel et al., 2012).While we currently have no
464 information on the acid-base balance within these larval crabs under prolonged exposure to steep
465 pCO_2 vertical gradients because no controlled experiments have been conducted, we propose
466 future studies to examine if internal dissolution could provide some level of bicarbonate ions for
467 buffering at comparatively low cost.

468 Alternative hypothesis for explaining internal dissolution might be based on the severity
469 of external dissolution extending much deeper (Figure S4) to initiate the endocuticle dissolution.
470 Once the dissolution of the external carapace dissolution is initiated, the mineralogical-elemental
471 structure of the mid- and endocuticle can allow for more rapid progression. The presence of
472 high-Mg^{2+} content in the endocuticle can cause more rapid dissolution (Andersson et al., 2008),
473 while comparatively lower Ca^{2+} content on the outward side presumably results in a weaker

474 carapace (Chen et al., 2008). In addition, chitin-proteinaceous matrix, such as an amorphous
475 crystalline layer might be present, which could importantly contribute to additional dissolution.
476 Furthermore, while the internal solubility extent may be compensated by phosphorus, it can
477 increase hardness, thereby preventing propagation of fractures, and Sr^{2+} because it can replace
478 Ca^{2+} in the mineralization process (Dodd, 1964). In contrast, the observation of less internal
479 dissolution on the endocuticle side compared to the external dissolution could be due to a
480 difference in biomineral composition. For instance, intermixing calcite in the endocuticle with
481 organic polymers would create a durable, protective covering, which may prevent the more
482 soluble high-Mg calcite in the endocuticle from dissolving (Chen et al., 2008). However, we
483 have no observations of dissolution penetration all the way from the external to the internal side,
484 we thus propose an acid-base balance strategy to be more feasible explanation for the internal
485 dissolution.

486

487 ***Potential detrimental effect associated with carapace dissolution***

488 One of the most important findings of this study is the correlation between carapace dissolution
489 and the reduction in larval width. This could, overtime, potentially impact population dynamics.
490 We suggest that the dissolution-length linkage could be explained by two different hypotheses:
491 first, pronounced dissolution under severe $\Delta\Omega_{cal,60}$ vertical gradients results in dissolution rate
492 outpacing calcification rate. In this mismatch of rates of two different processes, calcification
493 rate cannot fully compensate for dissolution and results in overall smaller width (‘*the mismatch’*
494 hypothesis). Alternatively, there could be an energetic implication behind the dissolution-
495 induced slowdown in width. In this form of the hypothesis, an organism expends additional

energy to increase calcification to counteract dissolution, thus resulting in an energetic trade-off that potentially compromises organismal growth (the '*trade-off*' hypothesis).

Furthermore, for early Dungeness crab life stages in the near-future, the prediction of more frequent and prolonged exposures to more severe $\Delta\Omega_{cal,60}$ gradients (Turi et al., 2016) could have potentially deleterious consequences in terms of behavioral and sensory impairments and chelae function. First, dissolution-affected thinner structures may become too weak to retain their integrity, particularly under more severe conditions and continuous water flow, resulting in ridged, puffed surfaces. Morphological changes may in turn negatively impact larval survival by altering swimming behaviors and competence, including the ability to regulate buoyancy, maintain vertical position, and avoid predators (Morgan, 1989; Sulkin, 1984). Similar morphological structures as those observed in our study were noted in the larval form of the European lobster (Agnalt et al., 2013), which under prolonged exposure to OA conditions led to irreparable carapace deformities, and these could lead to an increase in molt-related mortalities (Small et al.,2016). Second, dissolution on both sides of carapace and pereopod exoskeleton will inevitably limit the effectiveness of the exoskeleton in providing support for muscles contraction and defense from predators, aiding homeostatic functions, and enabling feeding functions. Third, calcified neuritic canals appear to be one of the dissolution hotspots compromising setae function. Compared with undamaged setae at undissolved surfaces (Figures 6 and S2, S3), dissolved areas may not provide sufficient structural integrity for the setae (Figure 6), potentially impairing their functionality. Given the role of setae as mechanoreceptors directly involved in supporting crustacean sensory and behavior processes, we hypothesize that the absence or damage of setae within their neuritic canals may in part provide a mechanistic understanding for potential aberrant behavioral patterns found across various crustacean species under low OA

519 conditions, such as slower movement, less tactile recognition, and prolonged searching time, as
520 well as impaired swimming (Alenius and Munguia, 2012; Dissanayake and Ishimatsu, 2011) and
521 behavioral choice (de la Haye et al., 2011). These changes can result in impaired competitiveness
522 and altered predator-prey relationships for crabs (de la Haye et al., 2012; Dodd et al., 2015;
523 Landes and Zimmer, 2012; Wang et al., 2018). Fourth, it is currently unknown whether external
524 dissolution in megalopae could carry over into later life stages, including the reproductively
525 active adult stage, and what the potential consequences may be for the population dynamics.
526 However, reduced calcification could result in poor mineralization through the intermolt period
527 that would be especially devastating for larval crabs because of potentially smaller sizes at
528 maturity, as well as increased vulnerability to predation during their most sensitive molting
529 stage.

530 While OA parameters largely affect observed biominerological and organismal
531 responses, population-level responses (i.e. abundances) are driven by food availability, with a
532 lesser role for temperature in the near-shore conditions. Although biological responses at
533 different levels of biological organization appear to be decoupled and responded to different
534 drivers across temporal and spatial scales that need to be taken into account to improve
535 biological forecasts and predictions. The only driver that seem to resonate across individual and
536 population level, at least marginally, is the temperature, which might have an opposite effect on
537 both levels. While warmer temperature negatively affects abundances, it also reduces internal
538 dissolution, although the latter is only a marginally significant.

539 To more accurately predict large-scale vulnerability, it is important to consider
540 population connectivity, related to essential population vital rates and affected by dispersal
541 (Lowe and Allendorf, 2010). This can be partitioned into genetic connectivity and demographic

connectivity, with our model outputs demonstrating onshore-offshore connectivity along the shelf-coastal and in the northern-southern directions. This implies prolonged exposure to less suitable habitats characterized by low $\Delta\Omega_{cal,60}$ in the nearshore areas that can exacerbate negative biological effects but some of them could be counteracted by higher food availability. With respect to genetic connectivity, the status of Dungeness crab as a high gene-flow species with low genetic differentiation along the US West Coast and the lack of significant adaptation patterns (Jackson and O'Malley, 2017; Jackson et al., 2018; O'Malley et al., 2017) implies that the genetic pool that might allow for adaptation under future climate scenario will be limited. This points toward the need for more comprehensive population vulnerability assessment that can link OA vulnerability with the population genetics.

Future Directions

Like dissolution in pteropods, larval dissolution observed in Dungeness crab is clear evidence that marine invertebrates are damaged by extended exposure to strong present-day OA-related vertical gradients in their natural environment. The unexplored aspect of OA impacts related to the damaged mechanoreceptors and potentially impaired sensory functions needs to be explored further. Namely, if the sensory functions are impaired, the transitioning from the larval to juvenile stage in their coastal habitat might be compromised under predicted scenarios of steeper ΔpH and $\Delta\Omega_{cal,60}$ gradients (Gruber et al., 2012; Turi et al., 2016). Multiple pathways of larval vulnerability should be studied in the context of carry-over effects to the next juvenile benthic stage to explore whether crustacean molting can offset some of the detrimental effects. Such findings should be integrated into a population demographic and exposure history model that could eventually lead to improved management of Dungeness crab stocks (Fernandes et al., 2017; Lam et al., 2016).

Acknowledgements: We thank Carry Weekes and Anna McLasky for collecting the larval individuals, Jennifer Fisher for providing guidance to Carry Weekes; Sten Littmann from Max Planck Institute in Bremen, Germany for elemental analyses. We are grateful to Polona Mrak and Miloš Vittori for analyses of the crab molting stages. We thank to Sandra Bigley for her editorial help with the manuscript.

Funding sources: This work was supported by the NOAA's Ocean Acidification Program for initial funding and NOAA Pacific Marine Environmental Laboratory (PMEL) for supporting NB, RAF, SRA, and SAS. This is PMEL contribution number 4906.

Competing financial interests: There were no competing financial interests.

References

Agnalt, A.-L., Grefsrud, E. S., Farestveit, M., Larsen, M., Keulder, F. (2013). Deformities in larvae and juvenile European lobster (*Homarus gammarus*) exposed to lower pH at two different temperatures. *Biogeosciences, 10*, 7883–7895.

Akaike, H. (1973). Information theory and an extension of the maximum likelihood principle. In: B. N. Petrov & F. Csaki (Eds.) Second International Symposium on Information Theory (pp. 267–281). Budapest, Hungary: Akademiai Kiado.

Alenius, B., Munguia, P. (2012). Effects of pH variability on the intertidal isopod, *Paradella dianae*. *Marine and Freshwater Behaviour and Physiology, 45*, 245–259.

585 Andersson, A. J., Mackenzie, F. T., Bates, N. R. (2008). Life on the margin: Implications of
586 ocean acidification on Mg-calcite, high latitude and cold-water marine calcifiers. *Marine*
587 *Ecology Progress Series, 373*, 265–273.

588 Bednaršek, N., Feely, R. A., Reum, J. C. P., Peterson, B., Menkel, J., Alin, S. R., Hales, B.
589 (2014). *Limacina helicina* shell dissolution as an indicator of declining habitat suitability
590 owing to ocean acidification in the California Current Ecosystem. *Proceedings of the Royal*
591 *Society B: Biological Sciences, 281*, 20140123.

592 Bednaršek, N., Feely, R. A., Tolimieri, N., Hermann, A. J., Siedlecki, S. A., Waldbusser, G. G.,
593 McElhany, P., Alin, S. R., Klinger, T., Moore-Maley, B., Pörtner, H. O. (2017). Exposure
594 history determines pteropod vulnerability to ocean acidification along the US West Coast.
595 *Scientific Reports, 7*, 4526.

596 Bednaršek, N., Johnson, J., Feely, R. A. (2016). Comment on Peck et al: Vulnerability of
597 pteropod (*Limacina helicina*) to ocean acidification: Shell dissolution occurs despite an
598 intact organic layer. *Deep-Sea Research Part II: Topical Studies in Oceanography, 127*, 53–
599 56.

600 Bednaršek, N., Ohman, M. D. (2015). Changes in pteropod distributions and shell dissolution
601 across a frontal system in the California Current System. *Marine Ecology Progress Series,*
602 *523*, 93–103.

603 Bednaršek, N., Tarling, G. A., Bakker, D. C., Fielding, S. , Cohen, A. , Kuzirian, A. , McCorkle,
604 D. , Lézé, B., Montagna, R. (2012). Description and quantification of pteropod shell
605 dissolution: A sensitive bioindicator of ocean acidification. *Global Change Biology, 18*,
606 2378–2388.

607 Busch, D. S., McElhany, P. (2016). Estimates of the direct effect of seawater pH on the survival
608 rate of species groups in the California Current Ecosystem. *PLoS One, 11*, e0160669.

609 Cameron, J. N. (1985). Compensation of hypercapnic acidosis in the aquatic blue crab,
610 *Callinectes sapidus*: the predominance of external sea water over carapace carbonate as the
611 proton sink. *Journal of Experimental Biology, 114*, 197–206.

612 Carter, B. R., Feely, R. A., Williams, N. L., Dickson, A. G., Fong, M. B., Takeshita, Y. (2018).
613 Updated methods for global locally interpolated estimation of alkalinity, pH, and nitrate.
614 *Limnology and Oceanography Methods, 16*(2), 119–131.

615 Chavez, F., Pennington, J. T., Michisaki, R. P., Blum, M., Chavez, G. M., Friederich, J., Messié,
616 M. (2017). Climate variability and change: Response of a coastal ocean ecosystem.
617 *Oceanography, 30*, 128–145.

618 Chen, P.-Y., Lin, A. Y.-M., McKittrick, J., Meyers, M. A. (2008). Structure and mechanical
619 properties of crab exoskeletons. *Acta Biomaterialia, 4*, 587–596.

620 Davis, S., Sylvia, G., Yochum, N., Cusack, C. (2017). Oregon Dungeness Crab Fishery
621 Bioeconomic Model: A Fishery Interactive Simulator Learning Tool. Version 5.7. Prepared
622 by Coastal Oregon Marine Experiment Station, Oregon State University and The Research
623 Group, LLC for the Oregon Dungeness Crab Commission.

624 de la Haye, K. L., Spicer, J. I., Widdicombe, S., Briffa, M. (2011). Reduced sea water pH
625 disrupts resource assessment and decision making in the hermit crab *Pagurus bernhardus*.
626 *Animal Behaviour, 82*, 495–501.

627 de la Haye, K. L., Spicer, J. I., Widdicombe, S., Briffa, M. (2012). Reduced pH sea water
628 disrupts chemo-responsive behaviour in an intertidal crustacean. *Journal of Experimental*
629 *Marine Biology and Ecology, 412*, 134–140.

630 Dissanayake, A., Ishimatsu, A. (2011). Synergistic effects of elevated CO_2 and temperature on
631 the metabolic scope and activity in a shallow-water coastal decapod (*Metapenaeus joyneri*;
632 Crustacea: Penaeidae). *ICES Journal of Marine Science, 68*, 1147–1154.

633 Dodd, J. R. (1964). Environmentally controlled variation in the shell structure of a pelecypod
634 species. *Journal of Paleontology, 38*, 1065–1071.

635 Dodd, L. F., Grabowski, J. H., Piehler, M. F., Westfield, I., Ries, J. B. (2015). Ocean
636 acidification impairs crab foraging behaviour. *Proceedings of the Royal Society B:*
637 *Biological Sciences, 282*, 20150333.

638 Fabritius, H. O., Karsten, E. S., Balasundaram, K., Hild, S., Huemer, K., Raabe, D. (2012).
639 Correlation of structure, composition and local mechanical properties in the dorsal carapace
640 of the edible crab *Cancer pagurus*. *Zeitschrift für Kristallographie, 227*(11), 766–776.

641 Feely, R. A., Alin, S., Carter, B., Bednaršek, N., Hales, B., Chan, F., …, L. Juranek (2016).
642 Chemical and biological impacts of ocean acidification along the west coast of North
643 America. *Estuarine, Coastal and Shelf Science, 183*, 260–270.

644 Feely, R. A., Okazaki, R. R., Cai, W.-J., Bednaršek, N., Alin, S. R., Byrne, R. H., Fassbender, A.
645 (2018). The combined effects of acidification and hypoxia on pH and aragonite saturation in
646 the coastal waters of the California current ecosystem and the northern Gulf of Mexico.
647 *Continental Shelf Research, 152*, 50–60.

Fernandes, J. A., Papathanasopoulou, E. , Hattam, C. , Queirós, A. M., Cheung, W. W., Yool, A., Artioli, Y. , Pope, E. C., Flynn, K. J., Merino, G. , Calosi, P. , Beaumont, N. , Austen, M. C., Widdicombe, S., Barange, M. (2017). Estimating the ecological, economic and social impacts of ocean acidification and warming on UK fisheries. *Fish and Fisheries, 18*, 389–411.

Fox, J., Weisberg, S. (2011). An R Companion to Applied Regression. USA: SAGE Publications.

Giltz, S. M., Taylor, C.M. (2017). Reduced growth and survival in the larval Blue Crab *Callinectes sapidus* under predicted ocean acidification. *Journal of Shellfish Research, 36*, 481–485.

González-Gordillo, J. I., Rodríguez, A., Queiroga, H. (2004). Characterization of the megalopal premoult stages of the Green crab, *Carcinus Maenas* (Decapoda, Portunidae), from laboratory culture. *Journal of Crustacean Biology, 24*, 502–510.

Gravinese, P. M., Enochs, I. C., Manzello, D. P., van Woesik, R. (2018). Warming and pCO_2 effects on Florida stone crab larvae. *Estuarine, Coastal and Shelf Science, 204*, 193–201.

Gruber, N., Hauri, C., Lachkar, Z., Loher, D., Frölicher, T. L., Plattner, G.-K. (2012). Rapid progression of ocean acidification in the California Current System. *Science, 337*, 220–223.

Hans, S., Fehsenfeld, S., Treberg, J. R., Weihrauch, D. (2014). Acid–base regulation in the Dungeness crab (*Metacarcinus magister*). *Marine Biology, 161*, 1179–1193.

Henry, R. P., Kormanik, G. A., Smatresk, N. J., Cameron, J. N. (1981). The role of $CaCO_3$ dissolution as a source of HCO_3^- for the buffering of hypercapnic acidosis in aquatic and terrestrial decapod crustaceans. *Journal of Experimental Biology, 94*, 269–274.

Hobbs, R. C., Botsford, L. W., Thomas, A. (1992). Influence of hydrographic conditions and wind forcing on the distribution and abundance of Dungeness crab, *Cancer magister*, larvae. *Canadian Journal of Fisheries and Aquatic Sciences, 49*, 1379–1388.

Hodgson, E. E., Kaplan, I. C., Marshall, K. N., Leonard, J., Essington, T. E., Busch, D. S., Fulton, E. A., Harvey, C. J., Hermann, A. J., McElhany, P. (2018). Consequences of spatially variable ocean acidification in the California Current: Lower pH drives strongest declines in benthic species in southern regions while greatest economic impacts occur in northern regions. *Ecological Modelling, 383*, 106–117.

Jackson, T. M., O'Malley, K. G. (2017). Comparing genetic connectivity among Dungeness crab (*Cancer magister*) inhabiting Puget Sound and coastal Washington. *Marine Biology, 164*(6), 123.

Jackson, T. M., Roegner, G. C., O'Malley, K. G. (2018). Evidence for interannual variation in genetic structure of Dungeness crab (*Cancer magister*) along the California Current System. *Molecular Ecology, 27*(2), 352–368.

Kaplan, I. C., Williams, G. D., Bond, N. A., Hermann, A. J., Siedlecki, S. A. (2016). Cloudy with a chance of sardines: Forecasting sardine distributions using regional climate models. *Fisheries Oceanography, 25*, 15–27.

Kunkel, J. G., Nagel, W., Jercinovic, M. J. (2012). Mineral fine structure of the American lobster cuticle. *Journal of Shellfish Research, 31*, 515–526.

Lam, V. W. Y., Cheung, W. W. L., Reygondeau, G., Sumaila, U. R. (2016). Projected change in global fisheries revenues under climate change. *Scientific Reports, 6*, 32607.

691 Landes, A., Zimmer, M. (2012). Acidification and warming affect both a calcifying predator and
692 prey, but not their interaction. *Marine Ecology Progress Series, 450*, 1–10.

693 Lindinger, M. I., Lauren, D. J., Mcdonald, D. G. (1984). Acid-base balance in the sea mussel,
694 *Mytilus edulis*. III. Effects of environmental hypercapnia on intra- and extracellular acid-base
695 balance. *Marine Biology Letters, 5*, 371–381.

696 Long, W. C., Swiney, K. M., Foy, R. J. (2016). Effects of high pCO_2 on Tanner crab
697 reproduction and early life history, Part II: Carryover effects on larvae from oogenesis and
698 embryogenesis are stronger than direct effects. *ICES Journal of Marine Science, 73*(3), 836–
699 848.

700 Lowe, W. H., Allendorf, F. W. (2010). What can genetics tell us about population connectivity?.
701 *Molecular Ecology, 19*, 3038–3051.

702 Manno, C., Rumolo, P., Barra, M., d'Albero, S., Basilone, G., Genovese, S., Mazzola, S.,
703 Bonanno, A. (2019). Condition of pteropod shells near a volcanic CO_2 vent region. *Marine*
704 *Environmental Research, 143*, 39–48.

705 Melzner, F., Gutowska, M. A., Langenbuch, M., Dupont, S., Lucassen, M., Thorndyke, M. C.,
706 Bleich, M., Pörtner, H. O. (2009). Physiological basis for high CO_2 tolerance in marine
707 ectothermic animals: Pre-adaptation through lifestyle and ontogeny? *Biogeosciences, 6*(3),
708 4693–4738.

709 Michaelidis, B., Ouzounis, C., Paleras, A., Pörtner, H. (2005). Effects of long-term moderate
710 hypercapnia on acid-base balance and growth rate in marine mussels *Mytilus*
711 *galloprovincialis*. *Marine Ecology Progress Series, 293*, 109–118.

712 Miller, J. J., Maher, M., Bohaboy, E., Friedman, C. S., McElhany, P. (2016). Exposure to low pH
713 reduces survival and delays development in early life stages of Dungeness crab (*Cancer*
714 *magister*). *Marine Biology, 163*, 118.

715 Morgan, S. G. (1989). Adaptive significance of spination in estuarine crab Zoeae. *Ecology, 70*,
716 464–482. https://doi.org/10.2307/1937551

717 North, E. W., Schlag, Z., Hood, R. R., Li, M., Zhong, L., Gross, T., Kennedy, V. S. (2008).
718 Vertical swimming behavior influences the dispersal of simulated oyster larvae in a coupled
719 particle-tracking and hydrodynamic model of Chesapeake Bay. *Marine Ecology Progress*
720 *Series, 359*, 99–115.

721 North, E. W., Adams, E. E., Schlag, Z., Sherwood, C. R., He, R., Hyun, K. H., Socolofsky, S. A.
722 (2011). Simulating oil droplet dispersal from the *Deepwater Horizon* spill with a Lagrangian
723 approach. In Y. Liu, A. Macfadyen, Z. Ji, & R. H. Weisberg (Eds.), Monitoring and
724 Modeling the Deepwater Horizon Oil Spill: A Record Breaking Enterprise. *Geophysical*
725 *Monograph Series* (pp. 217–226). USA: American Geophysical Union.

726 Norton, E., Siedlecki, S.A., Kaplan, I.C., Hermann, A.J., Fisher, J., Morgan, C., Officer, S.,
727 Saenger, C., Alin, S.A., Newton, J.A., Bednaršek, N., and Feely, R.A. (*in revision*). The
728 importance of environmental exposure history in forecasting Dungeness crab megalopae
729 occurrence using J-SCOPE, a high-resolution model for the US Pacific Northwest. *Frontiers*
730 *in Marine Science*

731 Oksanen, J., Blanchet, F. G., Friendly, M., Kindt, R., Legendre, P., McGlinn, D., Wagner, H.
732 (2019). Vegan: Community Ecology Package. R package version 2.5-5. Available at
733 https://CRAN.R-project.org/package=vegan.

O'Malley, K. G., Corbett, K., Beacham, T. D., Jacobson, D. P., Jackson, T. M., Roegner, G. C. (2017). Genetic connectivity of the Dungeness crab (*Cancer magister*) across oceanographic regimes. *Journal of Shellfish Research, 36*(2), 453–465.

Pacific States Marine Fisheries Commission (2019). Species Report: Commercial Land Catch: Metric-Tons (mt), Revenue, and Price-per-pound (Price/lbs). Portland, OR: Pacific States Marine Fisheries Commission. Available at https://reports.psmfc.org/pacfin/f?p=501:1:5808950816361::NO::: Accessed 3/25/2019.

Paganini, A. W., Miller, N. A, Stillman, J. H. (2014). Temperature and acidification variability reduce physiological performance in the intertidal zone porcelain crab *Petrolisthes cinctipes*. *Journal of Experimental Biology, 217*(22), 3974–3980.

Page, T. M., Worthington, S., Calosi, P., Stillman, J. H. (2016). Effects of elevated pCO_2 on crab survival and exoskeleton composition depend on shell function and species distribution: A comparative analysis of carapace and claw mineralogy across four porcelain crab species from different habitats. *ICES Journal of Marine Science, 74*(4), 1021–1032.

Pane, E., Barry, J. (2007). Extracellular acid-base regulation during short-term hypercapnia is effective in a shallow-water crab, but ineffective in a deep-sea crab. *Marine Ecology Progress Series, 334*, 1–9.

R Core Team (2019). R: A Language and Environment for Statistical Computing. R Foundation for Statistical Computing. Available at https://www.R-project.org/.

Schiffer, M., Harms, L., Pörtner, H., Mark, F., Storch, D. (2014). Pre-hatching seawater pCO_2 affects development and survival of zoea stages of Arctic spider crab *Hyas araneus*. *Marine Ecology Progress Series, 501*, 127–139.

Schlag, Z. R., North, E. W. (2012). Lagrangian TRANSport model (LTRANS v.2) User's Guide. Cambridge, Maryland: University of Maryland Center for Environmental Science, Horn Point Laboratory.

Shanks, A. L. (1995). Mechanisms of cross-shelf dispersal of larval invertebrates and fish. In: L. R. McEdward (Ed.), Ecology of Marine Invertebrate Larvae (pp. 324–367). USA: CRC Press.

Siedlecki, S. A., Kaplan, I. C., Hermann, A. J., Nguyen, T. T., Bond, N. A., Newton, J. A., Williams, G. D., Peterson, W. T., Alin, S. R., Feely, R. A. (2016). Experiments with seasonal forecasts of ocean conditions for the northern region of the California Current upwelling system. *Scientific Reports, 6*, 27203.

Sinclair, M. (1988). Marine Populations: An Essay on Population Regulation and Speciation. Washington Sea Grant. Seattle, Washington: University of Washington Press.

Small, D. P., Calosi, P., Boothroyd, D., Widdicombe, S., Spicer, J. I. (2015). Stage-specific changes in physiological and life-history responses to elevated temperature and pCO_2 during the larval development of the European lobster *Homarus gammarus* (L.). *Physiological and Biochemical Zoology*, *88*, 494–507.

Small, D. P., Calosi, P., Boothroyd, D., Widdicombe, S., Spicer, J. I. (2016). The sensitivity of the early benthic juvenile stage of the European lobster *Homarus gammarus* (L.) to elevated pCO_2 and temperature. *Marine Biology, 163*, 53.

Somero, G. N. (1986). Protons, osmolytes, and fitness of internal milieu for protein function. *American Journal of Physiology–Regulatory, Integrative and Comparative Physiology, 251,* R197–R213.

778 Somero, G. N., Beers, J. M., Chan, F., Hill, T. M., Klinger, T., Litvin, S. Y. (2015). What
779 changes in the carbonate system, oxygen, and temperature portend for the northeastern
780 Pacific Ocean: A physiological perspective. *BioScience, 66*, 14–26.

781 Spicer, J. I., Taylor, A. C. (1987). Carbon dioxide transport and acid-base regulation in the blood
782 of the beach-hopper *Orchestia gammarellus* (Pallas) (Crustacea: Amphipoda). *Ophelia, 28*,
783 49–61.

784 Spicer, J. I., Raffo, A. (2007). Widdicombe, S., Influence of CO_2-related seawater acidification
785 on extracellular acid–base balance in the velvet swimming crab *Necora puber*. *Marine*
786 *Biology, 151*, 1117–1125.

787 Sulkin, S. D. (1984). Behavioral basis of depth regulation in the larvae of brachyuran crabs.
788 *Marine Ecology Progress Series, 15*, 181–205.

789 Trigg, S. A., McElhany, P., Maher, M., Perez, D., Busch, D. S., Nichols, K. M. (1 August 2019).
790 Uncovering mechanisms of global ocean change effects on the Dungeness crab (*Cancer*
791 *magister*) through metabolomics analysis. *BioRxiv*, 574798.

792 Truchot, J. P. (1979). Mechanisms of the compensation of blood respiratory acid-base
793 disturbances in the shore crab, *Carcinus maenas* (L.). *Journal of Experimental Zoology, 210,*
794 407–416.

795 Tunnicliffe, V., Davies, K. T., Butterfield, D. A., Embley, R. W., Rose, J. M., Chadwick Jr, W.
796 W. (2009). Survival of mussels in extremely acidic waters on a submarine volcano. *Nature*
797 *Geoscience, 2*, 344–348.

798 Turi, G., Lachkar, Z., Gruber, N., Münnich, M. (2016). Climatic modulation of recent trends in
799 ocean acidification in the California Current System. *Environmental Research Letters, 11*,
800 014007.

801 Walther, K., Anger, K., Pörtner, H. (2010). Effects of ocean acidification and warming on the
802 larval development of the spider crab *Hyas araneus* from different latitudes (54° vs. 79°N).
803 *Marine Ecology Progress Series, 417*, 159–170.

804 Wang, Y., Hu, M., Wu, F., Storch, D., Pörtner, H.-O. (2018). Elevated pCO_2 affects feeding
805 behavior and acute physiological response of the Brown Crab *Cancer pagurus*. *Frontiers in*
806 *Physiology, 9*,1164.

807

808

809

810

811

812

813

814 **Figures**

815 **Figure 1:** The cross sections of the Dungeness crab megalopae. Left panel (a): cross section of
816 carapace (with increasing numbers describing the transition from the thinner exo- (1) to thicker
817 endo-cuticle (6). Right panel (b): distribution of various elements (C-carbon-a; N-nitrogen-b;
818 Sr^{2+}- strontium-c; Mg^{2+}- magnesium-d; P-phosphor-e; S-sulphur-f; K-potassium-g, Ca^{2+}-

819 calcium-h). The more intense colors depict higher elemental concentration. Spectrum
820 and % content of selected elements in either carapace or pereopod exoskeleton (*a*). The
821 numbers in (*a*) coincide with the numbers in (*b*) that indicate the position within the carapace.

822 **Figure 2:** Interpolated $pCO_{2,60}$ (*a*), $\Delta\Omega_{cal,60}$ (*b*) and chlorophyll (*c*) conditions in the onshore and
823 offshore habitats along the US West Coast in June 2016. pCO_2 reflects the conditions at 60m
824 depth and $\Delta\Omega_{cal,60}$ indicates the difference between the surface and 60 m depth. *c*) Chlorophyll
825 distribution and concentration (chl-a; µg/L) demonstrate an order of magnitude difference
826 between the regional nearshore and offshore region. The numbers indicate the stations at which
827 the crabs were collected.

828 **Figure 3**: Correlation matrix of environmental variables with biological endpoints for Dungeness
829 megalopae: *(a*) Darker green values are strong positive correlations and darker purple values are
830 strong negative correlations, while dimmer green and purple indicate weaker correlations; and *b*)
831 Redundancy analyses (RDAs) for environmental variables used in the analyses with crab
832 biological measurements (internal and external dissolution, carapace width).

833 **Figure 4:** External carapace and pereopod exoskeleton of the Dungeness crab megalopae (*a*) in
834 its undamaged form (*b, c*) and with dissolution presence ranging from mild (Stage 1; *d*) to severe
835 (Stage 2; *e, f*) patterns showing similarity in the structural damages (*g*) or exposed crystals (*h*).
836 Indicated is the scale of the measurements (µm). The undamaged megalopae originated from the
837 offshore or northwards habitats characterized by low $\Delta\Omega_{cal,60}$ vertical gradients, while the most
838 severely affected megalopae came from the nearshore or coastal habitats with steep $\Delta\Omega_{cal,60}$
839 conditions. See more detailed explanation of the exoskeleton dissolution in the Supplementary
840 Figures S2, S3.

841 **Figure 5:** Estimated linear relationships between ocean-acidification conditions and dissolution.
842 Specifically for *a*) $\Delta\Omega_{cal,60}$ and relative external dissolution ($R^2 = 0.87$; $p < 0.001$) with the
843 equation of relative external dissolution = $0.181*\Delta\Omega_{cal,60} + 0.215$; *b*) Depth-integrated $pCO_{2,60}$
844 and relative internal dissolution ($R^2 = 0.41$; $p = 0.064$); *c*) Comparison of the relative external
845 and internal dissolution ($R^2 = 0.24$; $p = 0.18$); and *d*) Relative external dissolution and carapace
846 width ($R^2 = 0.57$; $p = 0.08$). Dotted lines show the linear regression fit between all points. The
847 solid line in (*c*) is the 1:1 line and the green line in (*d*) is the regression fit only through the
848 onshore points. See methods for explanation of the term relative dissolution. Carapace width is in
849 mm.

850 **Figure 6**: Presence of setae on the pereopods (*a*) and carapace surface (*b*) of the megalopae on
851 the intact individuals. The exposure to greater $\Delta\Omega_{cal,60}$ differences mechanically damages the
852 setae and results in their absence and outrooting (black squares) because of the dissolution
853 around the neuritic canals (*d*, *f*) and damage with the collapsed structure (*e*).

854 **Figure 7:** Particle initialization locations (*a*) and average backtracked locations (*b*-*e*) for 7, 14,
855 21, and 30-day simulated particles exhibiting diel vertical migration (DVM) between 0 and 60 m
856 depths. Replicate particles (n=100) were initialized in the model at 51 locations representing the
857 sampling stations for the 2016 West Coast Ocean Acidification Cruise. J-SCOPE's historical
858 simulation of ocean conditions for 2016 was used to simulate advection of particles, and each
859 particle exhibited vertical swimming between the ocean surface at night and a maximum daytime
860 depth of 60 m. On a weekly basis, particle locations were averaged for all 100 particles
861 initialized at the same station, which sometimes resulted in the average location being on land.
862 These particles were moved to the nearest shoreline. Station color varies by transect for

863 improved resolution of dispersal patterns occurring at different latitudes. The 200 m isobath is
864 shown for reference, and land is shaded in grey.

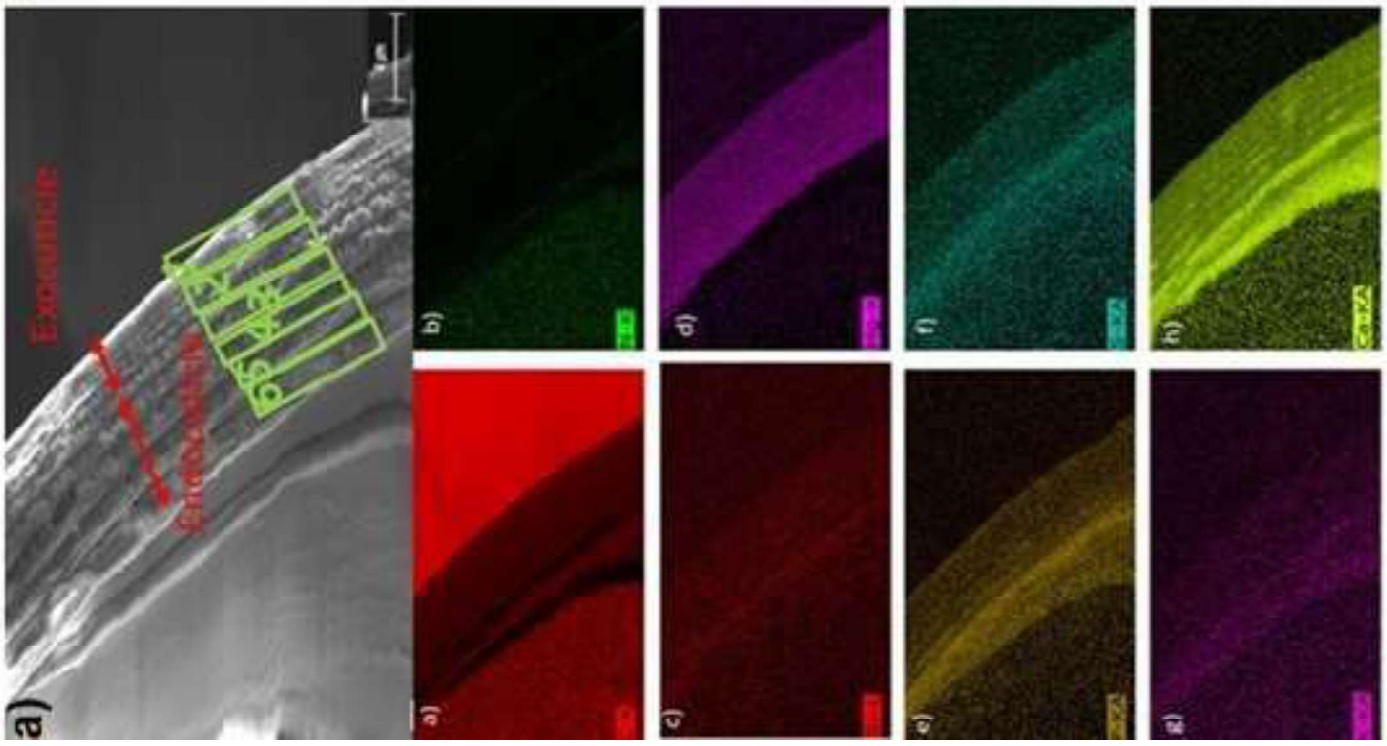

Figure 1
Click here to download high resolution image

Figure 2

Click here to download Figure: Fig2_total_final.pdf

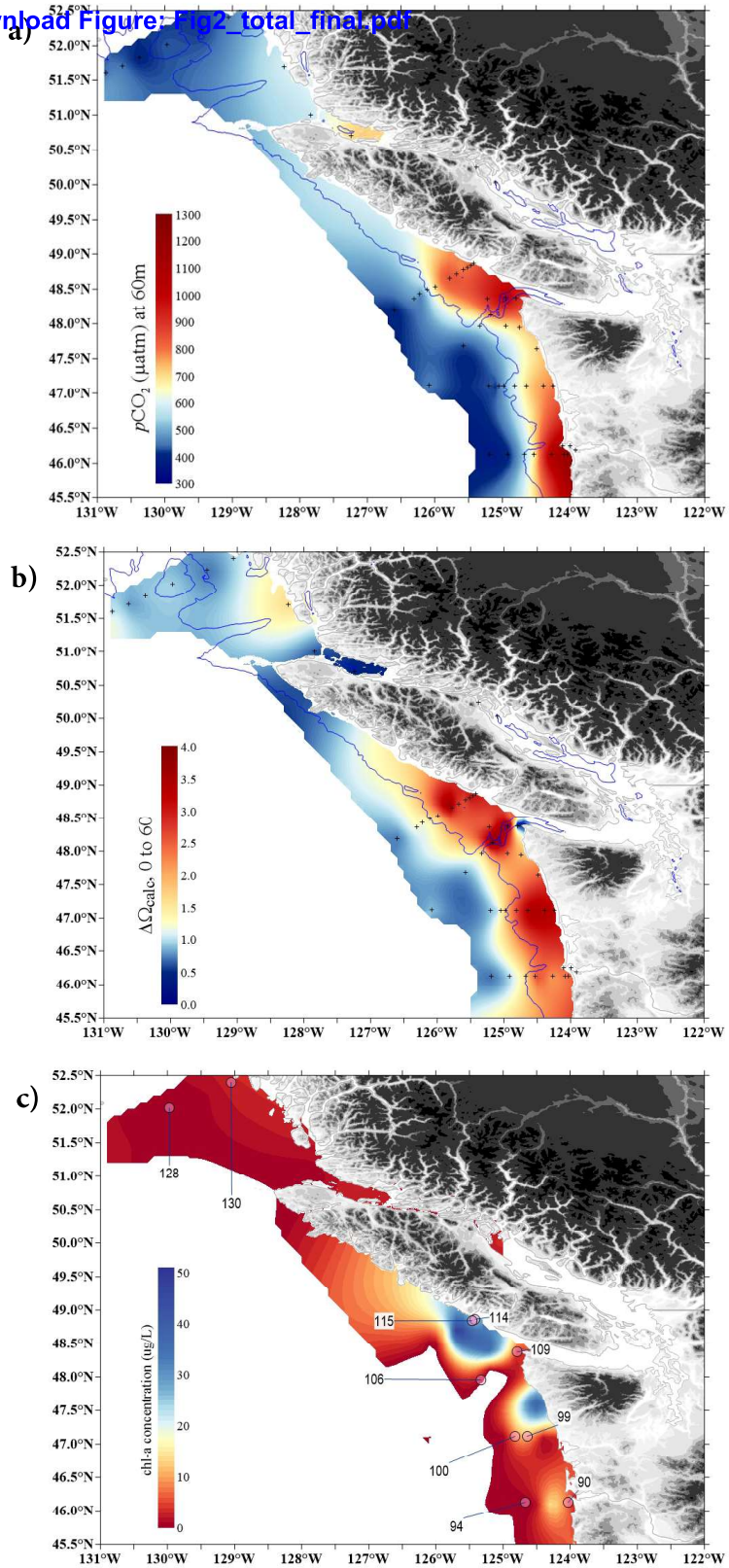

Figure 3a
Click here to download high resolution image

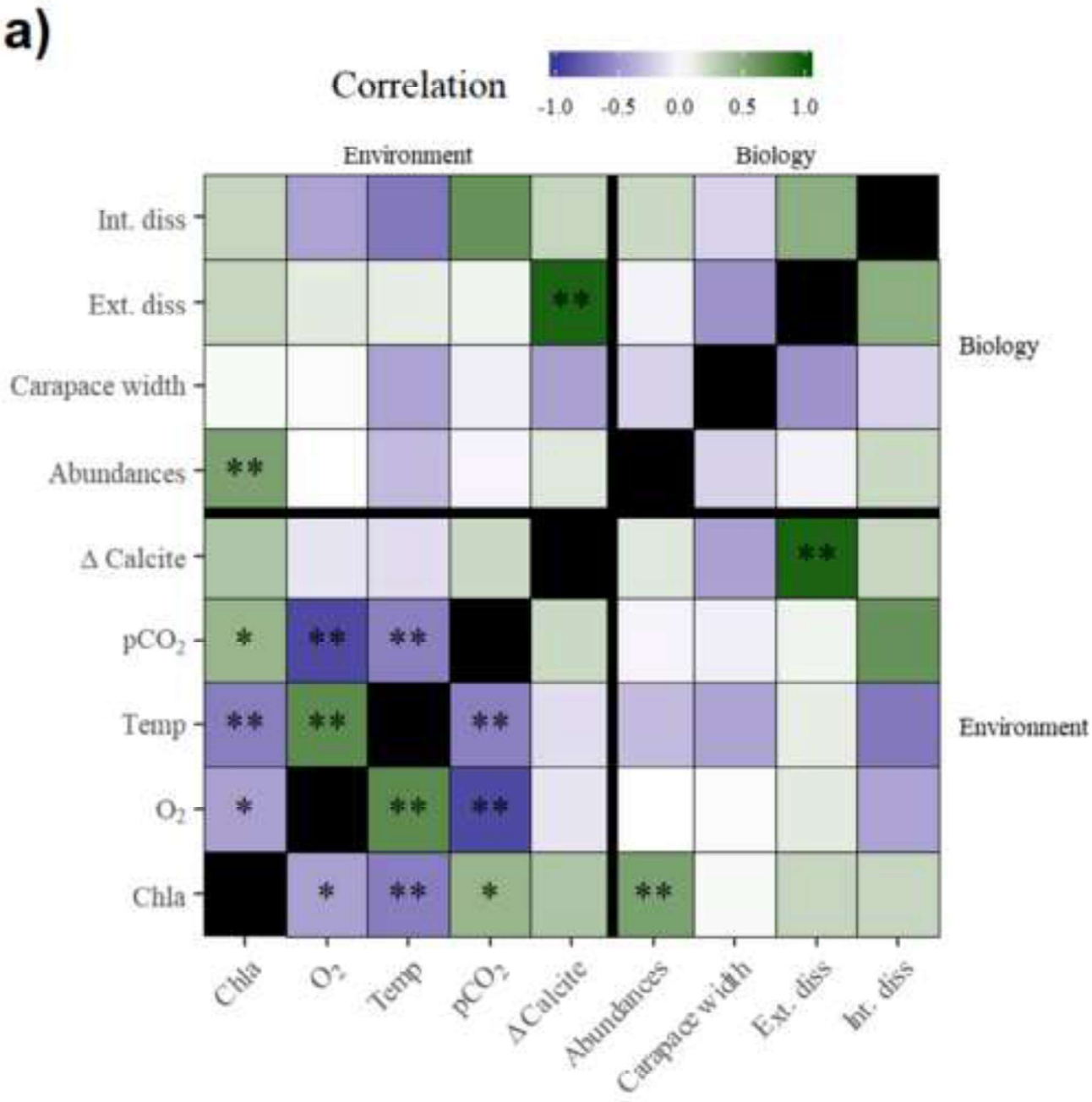

Figure 3b
Click here to download high resolution image

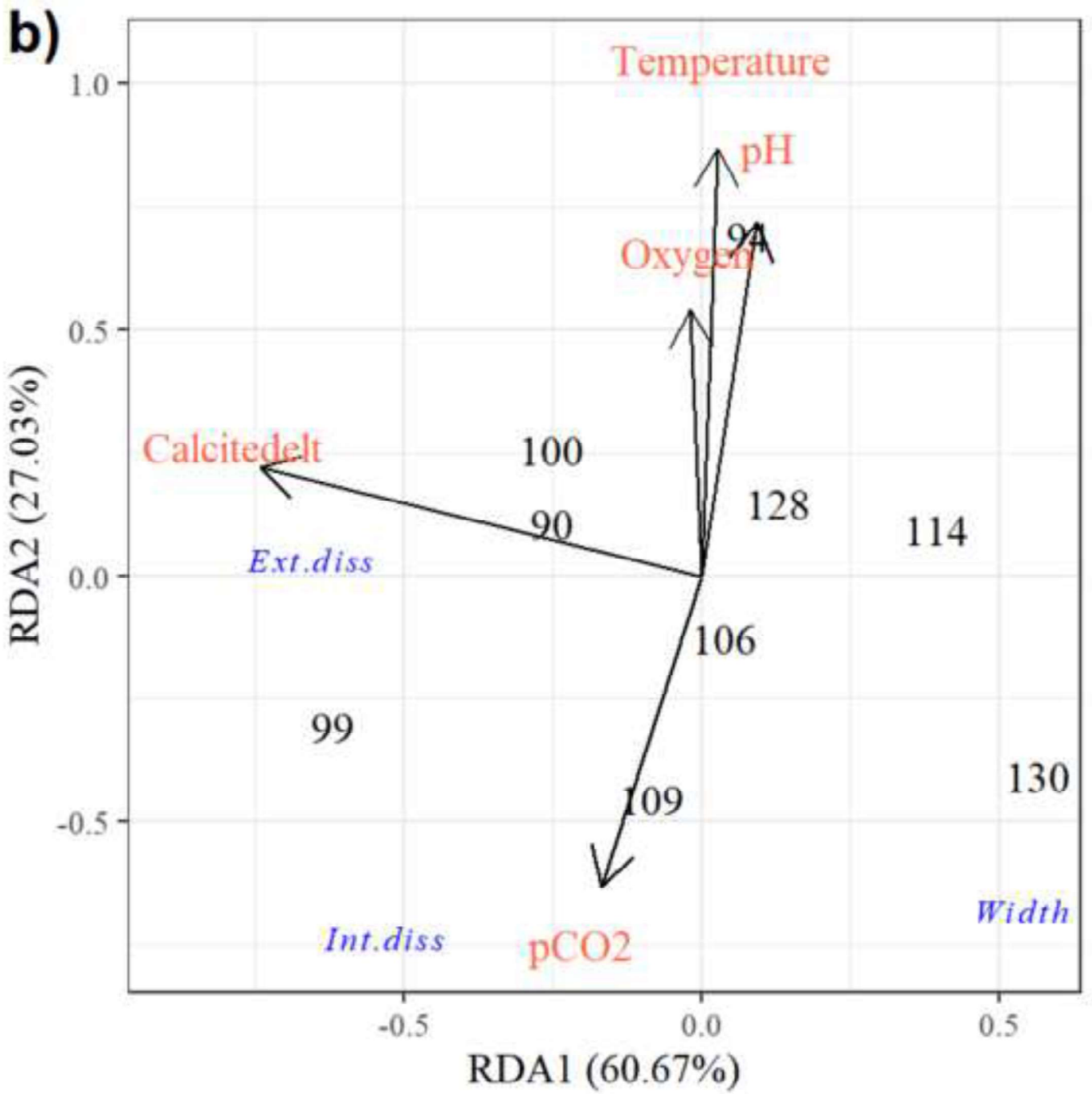

Figure 4

Click here to download high resolution image

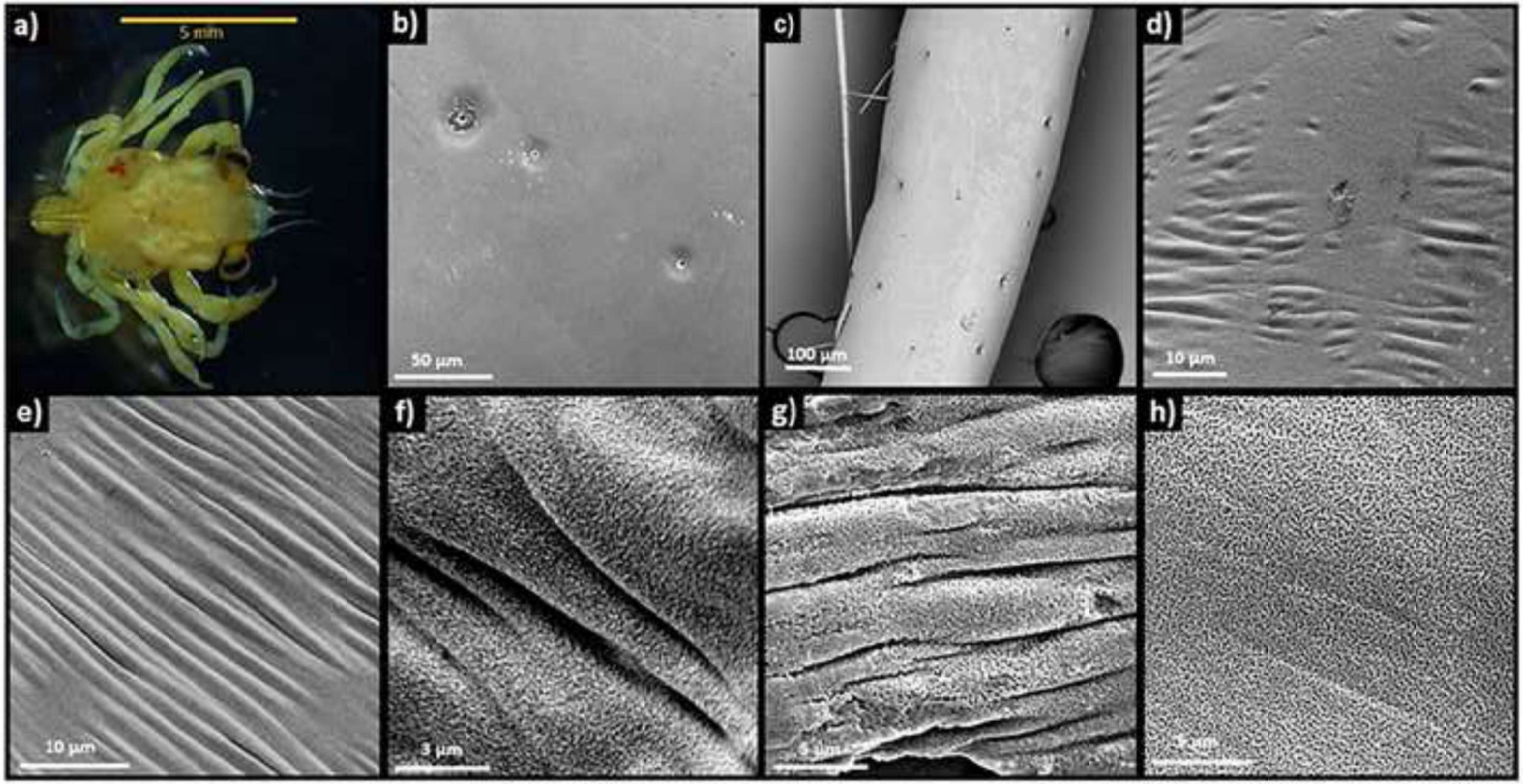

Figure 5
Click here to download high resolution image

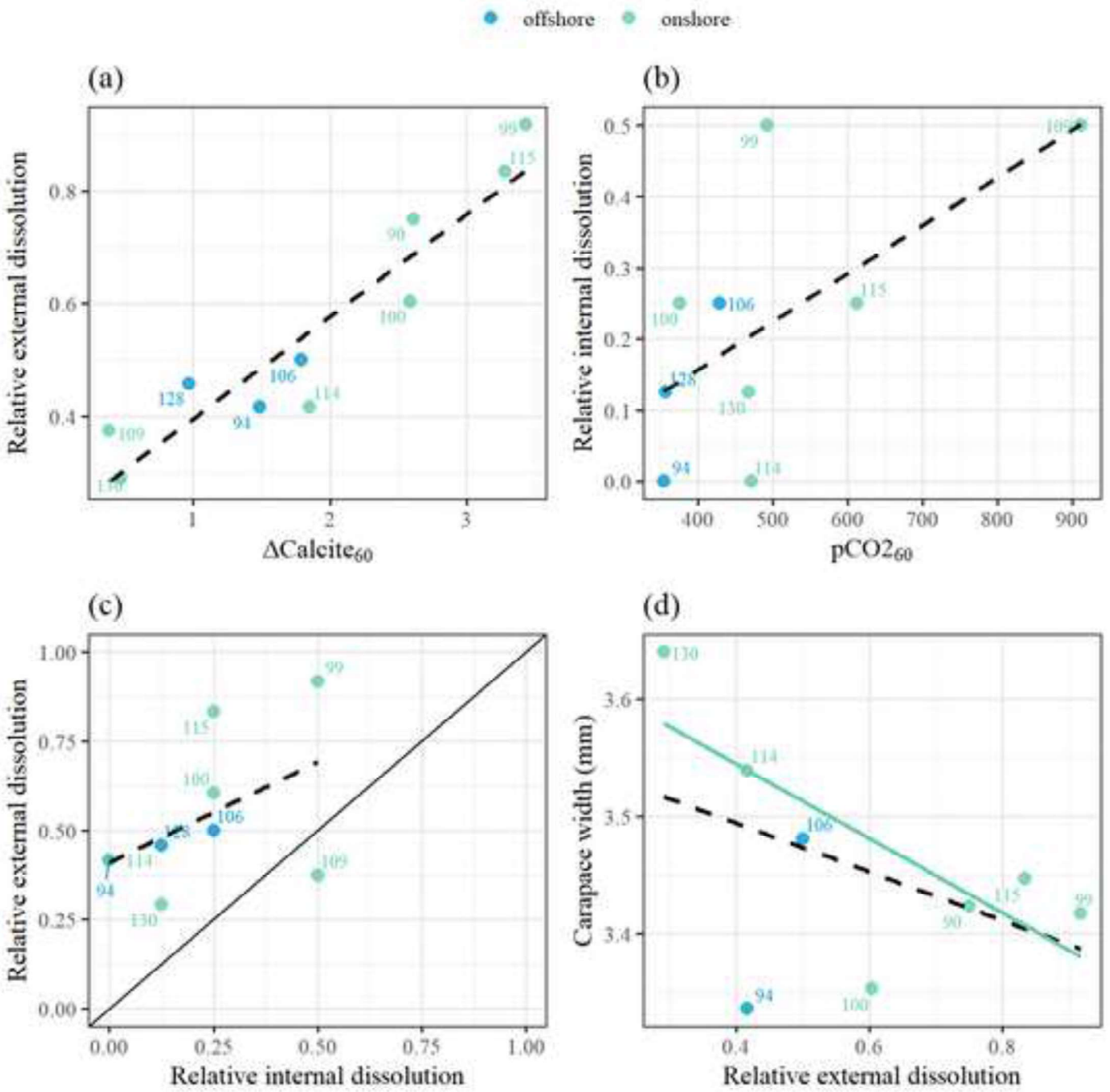

Figure 6

Click here to download high resolution image

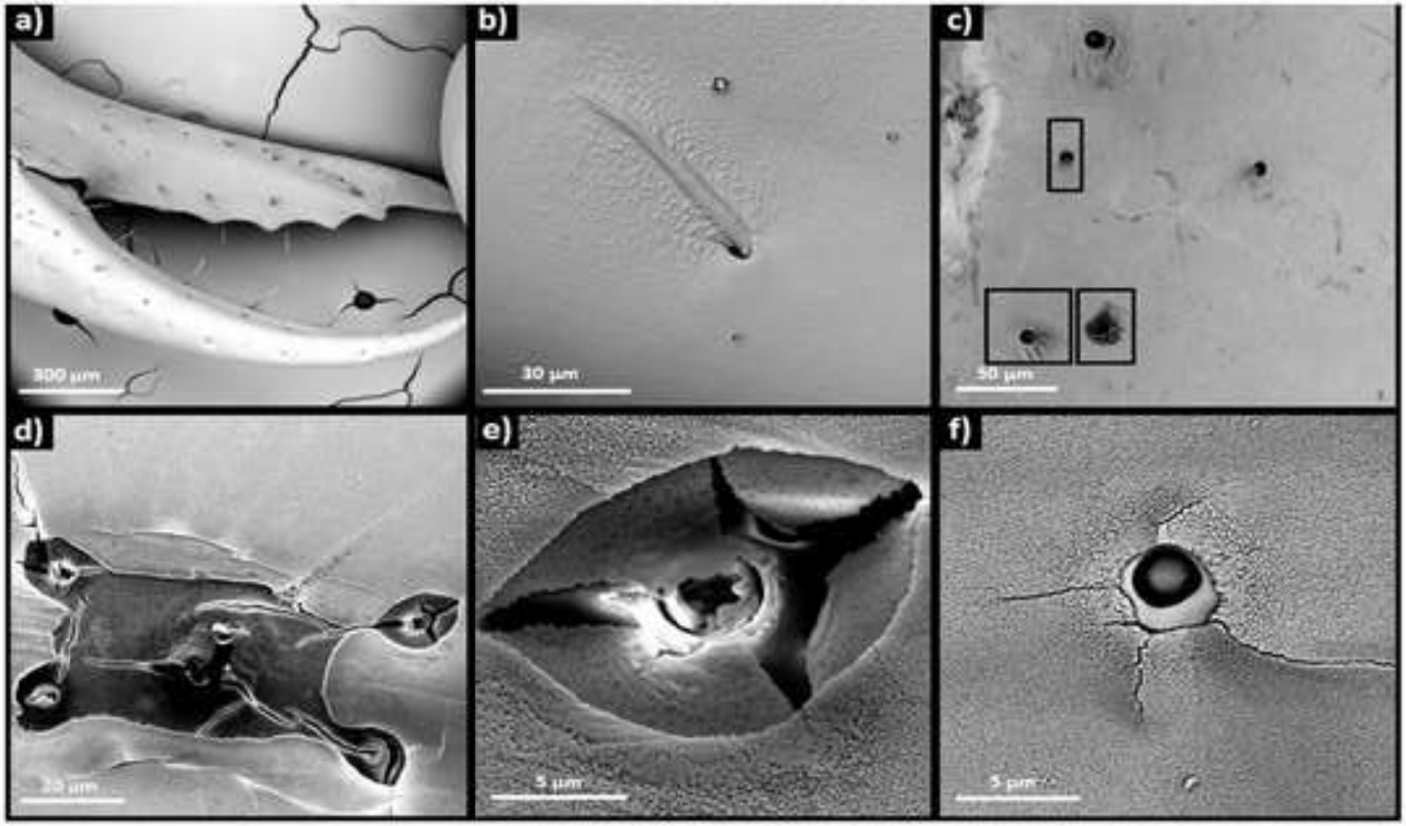

Figure 7

Click here to download high resolution image